SPACE TELESCOPE SCIENCE INSTITUTE
Operated for NASA by AURA

Instrument Science Report WFC3 2014-20

Update on the WFC3/UVIS Stability and Contamination Monitor

C. M. Gosmeyer, S. Baggett, S. Deustua, D.M. Hammer

September 10, 2014

Abstract

The photometric throughput of WFC3 is measured periodically throughout the year to evaluate its stability as a function of time and wavelength, as well as to check for the presence of possible contaminants in the UVIS channel. These monitoring data consist of observations of the white dwarf spectrophotometric standard GRW+70d5824, taken in a subset of key filters covering 200-600 nm, with F606W and F814W acting as controls on the red end. Here we analyze the observations from 2009 to mid-2014. No contamination effects have been detected, though small photometric drifts are evident: a slight increase in throughput in the UV filters (∼0.1%/year) and slight decreases in throughput in red and visible filters (∼0.2%/year and 0.4%/year, respectively).

1. Introduction

Stability is one of the Hubble Space Telescope's greatest strengths over ground-based observatories. Because of this stability, Hubble's instruments allow for unparalleled characterization of a wide variety of astrophysical phenomena. In order to provide optimum calibration for all on-orbit observations, we need to evaluate the telescope and instruments'

spatial and temporal stability. Spatial stability can be assessed by looking for variations in the flat fields by measuring the count rates for the same star on different locations on the detector (see Sabbi 2009). Temporal stability can be assessed by periodic observations with high signal-to-noise of bright, isolated standard stars.

Since its installation in May 2009, we have had such a temporal stability monitoring program in place for the Wide Field Camera 3 (WFC3) instrument, for both its IR and its UVIS channel. Using a defined instrumental setup and cadence, this program images the standard star GRW+70D5824 in a subset of the UVIS and IR filters, as well as the UVIS grism, to monitor the temporal stability of WFC3, detect possible contamination in the UV filters, and, in conjunction with other programs, determine photometric zeropoints. We can propagate any changes into the SYNPHOT files, which are used to provide flux calibration for science data.

The UVIS channel, the focus of this report, covers the 200-1000nm spectral range and consists of two 2K×4K CCD chips, 62 filters, and one grism. Because the two CCD chips were manufactured on different wafers, there are differences in the two chips' properties and behaviors. Therefore, we treat the two chips separately in our characterizations of temporal stability and contamination.

2. The Dataset

The white dwarf spectrophotometric standard GRW+70D5824 has been observed periodically since the beginning of the WFC3 mission in mid-2009. Part of the original set of standard stars chosen for HST (Bohlin, 1996), GRW+70D5824 has been successfully used as a monitor on other instruments such as STIS (Stys et al., 2001) and WFPC2 (Whitmore et al., 1996). See Table 1 for characteristics and spectra of the star. Initially, observations were acquired about once a week; given the excellent performance of the instrument, the frequency of the photometric monitor has been gradually reduced to its present level, about once every five weeks. For our analysis we gathered GRW+70D5824 UVIS observations from the following programs.

- SMOV Proposal CAL11426 – "UVIS SMOV Contamination Monitor"
- Cycle 17 Proposal CAL11907 – "UVIS Cycle 17 Contamination Monitor"
- Cycle 18 Proposal CAL12333 – "UVIS Cycle 18 Photometric Monitor"
- Cycle 19 Proposal CAL12698 – "UVIS Cycle 19 Contamination and Photometric Stability Monitor"

- Cycle 20 Proposal CAL13088 – "WFC3 Contamination and Photometric Stability Monitor"
- Cycle 21 Proposal CAL13574 – "WFC3 Contamination and Stability Monitor"

Proposal CAL11426 samples two of the WFC3 mosaic's readout amplifiers (A and C) in 13 UV filters and proposal CAL11907 samples all four amplifiers in nine UV filters. Both take images in F606W and F814W to serve as controls. Proposals CAL12333, CAL12698, CAL13088, and CAL13574 sample only two amplifiers (A and C), using 14, 13, five, and five UV filters, respectively, again along with the controls F606W and F814W. This gives us a continuous coverage of data for five UV filters over almost five years. The filters cover the Narrow (N), Medium (M), Wide (W), and Long Pass (LP) bands.

We summarize our imaging data in Table 2. In Table 3 we give a more detailed list of exposure times for each filter in each epoch.

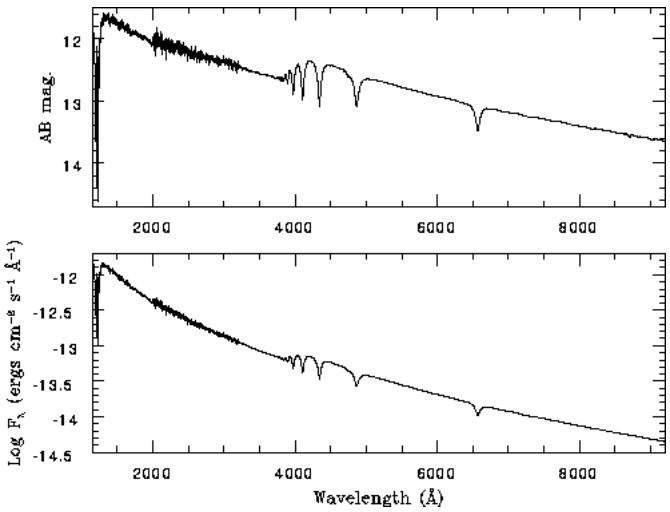

RA (2000)	*DEC* (2000)	*V mag*	$B-V$	*Spectral Type*
13h 38m 51.77s	+70d 17' 08.5"	12.77	-0.09	DA3

Table 1: *Characteristics of our white dwarf spectroscopic standard, GRW+70D5824. From the ESO RA Ordered List of Spectroscopic Standards,* `http://www.eso.org/sci/observing/tools/standards/spectra/stanlis.html`.

Prop. ID	*Epoch*	*Subarrays*	*Filters*	*Exp. Times (sec)*	*Post − flash?*
CAL11426	6/2009 – 8/2009	UVIS1-C512A-SUB, UVIS2-C512C-SUB	F218W, F225W, F275W, F280N, F336W, F343N, F373N, F390M, F390W, F395N, F410M, F438W, F467M, F606W, F814W	3.9, 1.4, 1.3, 23.8, 0.8, 1.6, 10.2, 2.1, 0.48, 5.3, 2.0, 0.48, 1.8, 0.48, 1.0	N
CAL11907	8/2009 – 10/2010	UVIS1-C512A-SUB, UVIS1-C512B-SUB, UVIS2-C512C-SUB, UVIS2-C512D-SUB	F218W, F225W, F275W, F336W, F390M, F390W, F438W, F475W, F547M, F606W, F814W	6.0, 2.0, 2.0, 1.5, 4.0, 1.0, 1.0, 1.0, 1.5, 0.48, 2.0	N
CAL12333	11/2010 – 10/2011	UVIS1-C512A-SUB, UVIS2-C512C-SUB	F218W, F225W, F275W, F336W, F390M, F390W, F438W, F467M, F469N, F475W, F502N, F547M, F555W, F606W, F814W, F850LP	17.6, 6.3, 6.0, 4.0, 11.0, 2.1, 3.1, 8.6, 48.0, 1.5, 33.4, 4.0, 1.5, 1.3, 6.2, 32.5	N
CAL12698	10/2011 – 10/2012	UVIS1-C512A-SUB, UVIS2-C512C-SUB	F218W, F225W, F275W, F336W, F390M, F390W, F438W, F467M, F475W, F502N, F547M, F555W, F606W, F814W, F850LP	17.6, 6.3, 6.0, 4.0, 11.0, 2.1, 3.1, 8.6, 1.5, 33.4, 4.0, 1.5, 1.3, 6.2, 32.5	N
CAL13088	11/2012 – 11/2013	UVIS1-C512A-SUB, UVIS2-C512C-SUB	F218W, F225W, F275W, F336W, F438W, F606W, F814W	17.6, 6.3, 6.0, 4.0, 3.1, 1.3, 6.2	Y
CAL13574	12/2013 – 3/2014	UVIS1-C512A-SUB, UVIS2-C512C-SUB	F218W, F225W, F275W, F336W, F438W, F606W, F814W	17.6, 6.3, 6.0, 4.0, 3.1, 1.3, 6.2	Y

Table 2: *The target is the white dwarf spectrophotometric standard GRW+70D5824 taken on WFC3/UVIS subarrays located on the corners of the UVIS two-chip mosaic with nominal gain 1.5. We have observations in a total of 19 UV filters, including F606W and F814W. The five UV filters critical for contamination assessment (F218W, F225W, F275W, F336W, F438W) were observed throughout the entire five-year period; other filters were observed less frequently. All proposals took observations in amplifier quadrants A and C. Only the early proposal CAL11907 took additional observations in quadrants B and D. The exposure times correspond to each filter listed in the same relative location. Post-flashing of observations began in proposal CAL13088, after the mode became available for use on-orbit. The current proposal, CAL13574, is to continue until October 2014.*

		Obs. Period	
Filter	*Exp. Time (sec)*	*Amps A & C*	*Amps B & D*
F218W	3.9	6/2009 – 8/2009	
	6.0	8/2009 – 10/2010	8/2009 – 10/2010
	17.6	11/2010 – 3/2014	
F225W	1.4	6/2009 – 8/2009	
	2.0	8/2009 – 10/2010	8/2009 – 10/2010
	6.3	11/2010 – 3/2014	
F275W	1.3	6/2009 – 8/2009	
	2.0	8/2009 – 10/2010	8/2009 – 10/2010
	6.0	11/2010 – 3/2014	
F280N	23.8	6/2009 – 8/2009	
F336W	0.8	6/2009 – 8/2009	
	1.5	8/2009 – 10/2010	8/2009 – 10/2010
	4.0	11/2010 – 3/2014	
F343N	1.6	6/2009 – 8/2009	
F373N	10.2	6/2009 – 8/2009	
F390M	2.1	6/2009 – 8/2009	
	4.0	8/2009 – 10/2010	8/2009 – 10/2010
	11.0	11/2010 – 10/2012	
F390W	0.48	6/2009 – 8/2009	
	1.0	8/2009 – 10/2010	8/2009 – 10/2010
	2.1	11/2010 – 10/2012	
F395N	5.3	6/2009 – 8/2009	
F410M	2.0	6/2009 – 8/2009	
F438W	0.48	6/2009 – 8/2009	
	1.0	8/2009 – 10/2010	8/2009 – 10/2010
	3.1	11/2010 – 3/2014	
F467M	1.8	6/2009 – 8/2009	
	8.6	11/2010 – 10/2012	
F469N	48.0	11/2010 – 10/2011	
F475W	1.0	8/2009 – 10/2010	8/2009 – 10/2010
	1.5	11/2010 – 10/2012	
F502N	33.4	11/2010 – 10/2011	
	33.4	10/2011 – 10/2012	
F547M	1.5	8/2009 – 10/2010	8/2009 – 10/2010
	4.0	11/2010 – 10/2012	
F555W	1.5	11/2010 – 10/2012	
F606W	0.48	6/2009 – 8/2009	
	0.48	8/2009 – 10/2010	8/2009 – 10/2010
	1.3	11/2010 – 3/2014	
F814W	1.0	6/2009 – 8/2009	
	2.0	8/2009 – 10/2010	8/2009 – 10/2010
	6.2	11/2010 – 3/2014	
F850LP	32.5	11/2010 – 10/2012	

Table 3: *Additional details of the exposure times for each filter in all periods the exposure time was used. Amplifiers B and D were observed only in one Cycle. See Table 2 for description of the observations.*

3. Photometry Analysis

Our data were taken from Mikulski Archive for Space Telescopes (MAST) versions that are kept in a local on-line archive. They were processed with the `IRAF/STSDAS` pipeline program `CALWF3` (Version 3.0 or later) and a common set of calibration files. The UVIS calibration has remained stable from Version 3.0 onward and the updates do not affect our point-source photometry. All of the observations we analyze here were obtained using a 512 pixel subarray, located on the corners of the WFC3 4k×4k mosaic. The two subarrays used on UVIS chip 1 are UVIS1-C512A-SUB and UVIS1-C512B-SUB and the two subarrays on UVIS chip 2 are UVIS2-C512C-SUB and UVIS2-C512D-SUB. See Figure 1. We use subarrays in order to minimize readout times and pack as many exposures into an orbit as possible. We use the four corners in order to sample all four amplifiers as well as widely-separated regions on the detector. Placement of the source close to the amplifier also reduces the adverse affects of charge transfer efficiency (CTE) decline due to on-orbit radiation damage. Only in proposal CAL11907 do we have data from all four amplifiers. In order to minimize the on-orbit time required for calibration, most proposals only use the subarrays located in amplifier quadrants A (on chip 1) and C (on chip 2). Early in the mission, exposure times were kept low (proposals CAL11426 and CAL11907) in order to avoid any possibility of saturation; they have since been increased where possible.

We perform our analysis on the `CALWF3`-processed `_flt` images. `CALWF3` applies bias, post-flash, and dark image subtraction, and flat-fielding and gain conversion. We correct the `_flt` images for geometric distortion using the pixel area map (available at `http://www.stsci.edu/hst/wfc3/pam/pixel_area_maps`) and remove cosmic rays using the `IRAF` version of the Laplacian edge detection program, `LACOSMIC` (see `http://www.astro.yale.edu/dokkum/lacosmic/` and Dokkum 2001). We are confident that our removal of cosmic rays using `LACOSMIC` is robust. For instance, Kalirai *et al*. (2010) compared the source count rate for images cleaned by dithering to the images cleaned by `LACOSMIC` and found that they agree to a small fraction of a percent. We do our own checks, as well: after we run `LACOSMIC`, we inspect each image for cosmic ray flags in the source star. If the pixels under the star are flagged, we discard the image. These over-flagged images account for less than 5% of our total dataset, and since we have many hundreds of images, we have not attempted to salvage the discarded images by correcting the cosmic rays manually.

We create a source list of our spectrophotometric standards with `IRAF/DAOFIND` and perform aperture photometry with `IRAF/PHOT` using 26 aperture radii ranging from 1 to 70 pixels. The sky is measured as the clipped mean of all the image's pixels, excluding a circle of 80 pixels from the source and a frame of 20 pixels following the image border.

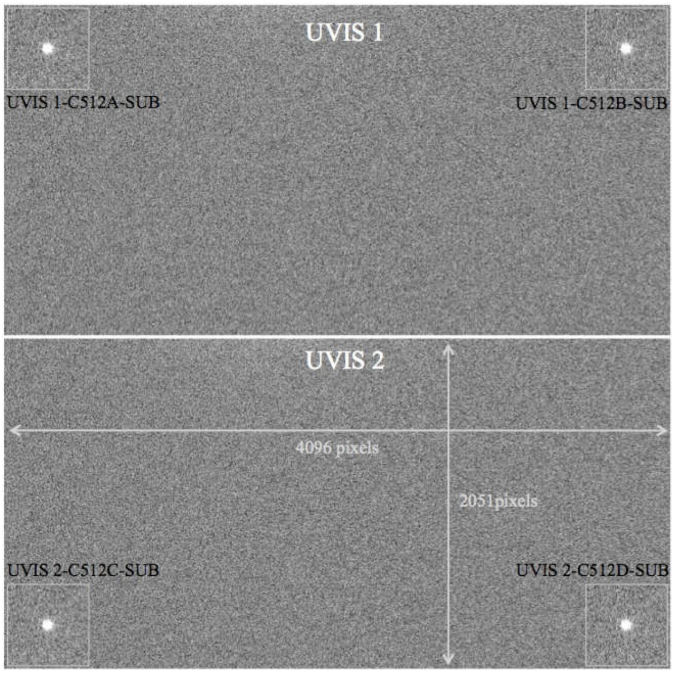

Fig. 1.— *The to-scale locations of the four corner 512 pixel subarrays on the WFC3 two-chip mosaic. We minimize the readout overheads and buffer dumps by imaging the standard star in these subarrays rather than in the full two chips. Figure from Kalirai et al. (2010).*

3.1. Comparing Post-Flashed with Non-Post-Flashed Observations

Due to radiation damage accumulated on-orbit, the charge transfer efficiency (CTE) of the detector degrades over time. CTE losses are most severe for faint targets and low image backgrounds (Noeske *et al.* 2012). Our images have low backgrounds because we used only short exposure times on our bright standard star. However, the standard star's brightness, its placement close to the readout amplifier, and the relatively large aperture work in our favor to minimize CTE losses. Nevertheless, starting in Proposal CAL13088 (early 2013), all our data are post-flashed to further mitigate any potential CTE losses. In order to provide a transitional cross-check with the nonflashed data from the previous cycle, one of the three F218W images and one of the three F225W images during the visit on 4 Feb. 2013 were left not post-flashed.

We compare the flux and sky background levels of these six observations in Figure 2. The number statistics are small but the plots show the fluxes agree to within 1%, with no indication of a jump from post-flash to non-post-flash, indicating that the `CALWF3` post-flash correction is robust. We find that `IRAF/LACOSMIC` tends to flag more pixels than necessary in the background of the post-flashed images, and this can lower the measured background

value slightly. We have, however, confirmed that the effect of the lower background on the final star flux is negligible (4^{-4} to 5^{-5}) since the total counts from the standard star within the aperture is large (>300,000 electrons).

We conclude that our flashed and nonflashed observations are consistent with each other.

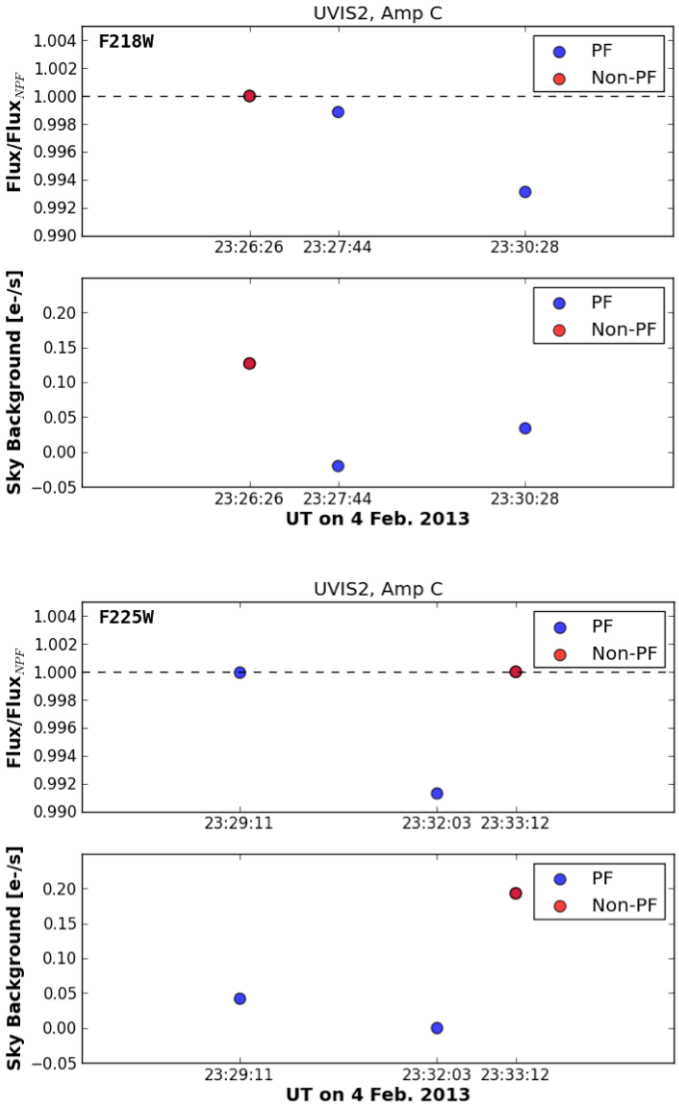

Fig. 2.— *Filter F218W is at top and F225W is at bottom. All six observations were taken in a single visit, and in each filter two observations were post-flashed and one observation not post-flashed. The top plots show the 10-pixel aperture flux (in e-) divided by the flux of the non-post-flashed observation. The bottom plots show the sky background (in e-/s) for each observation after bias, dark, and post-flash subtraction.*

4. Discussion

In our analysis, we examine the flux for a 10 pixel (0.4 arcsecond) aperture radius. Of the 19 UV filters for which we have data, 12 were always observed in subarrays UVIS1-C512A-SUB and UVIS2-C512C-SUB over the time period Nov. 2010 - Oct. 2012, and five of the 12 over the time period Nov. 2010 - Mar. 2014. We will, therefore, focus our analysis on these 12 filters.

For each observation, we obtain the countrate by dividing the total sky-corrected flux in electrons within the aperture by the exposure time. We then normalize each countrate to an average countrate determined from the first three images taken in the given filter and present the results as a percent difference ($\Delta Flux$). Standard error propagation (poisson) yields $\Delta Flux$ uncertainties in the early observations (when exposure times were shortest) of 3-5%. In the more recent observations, which have higher signal-to-noise, the uncertainties decrease to 2% or less. In Figures 3 and 4, we plot $\Delta Flux$ versus time for all observations taken in each filter, along with the derived linear fits obtained using `IRAF/TLINEAR`. A number of features are apparent, which we discuss in more detail below.

4.1. Scatter in Observations

Photometry from early in the mission (prior to 31 Oct. 2010, MJD <55500) shows larger scatter than later photometry, particularly in the UV filters but also apparent in F606W and F814W. Some of the effect is likely due to lower signal-to-noise in the shorter, conservative exposure times of the earlier data (error bars on the earlier data are 3-5%; more recent data have ∼2% error bars). We have investigated a number of other possibilities, listed below, but the cause of the overall scatter remains unknown.

- `LACOSMIC` incorrectly flagging and subtracting pixels from the source's PSF. We re-performed the photometry on images which had cosmic ray-cleaning applied only on the region outside 20 pixels from the source center. There were no significant changes in the countrates, except for a few individual outliers whose delta flux increased by 0.5-1.0. This test did, however, provide further validation of the `LACOSMIC` results.
- Pixel area map. We re-performed the photometry without applying the PAM correction. Again, the excursions in flux remain.
- Flatfield. We re-performed the photometry with non-flat fielded data. Some of the outliers do improve but other outliers appear, and the overall scatter is generally worse.

In addition to the overall scatter, the delta flux values in the blue filters on UVIS chip 1 also show sharp dips (>2%) at MJD∼55100 and MJD∼55450 (Aug. - Oct. 2009 and Aug. - Oct. 2010). These dips occur at the beginning and the end of proposal CAL11907. However, given that there was no change to the visit structure and observing sequence (the visits in question are identical to the visits throughout CAL11907), the timing of the dips in throughput with the proposal appears to be a red herring. Furthermore, there are other, albeit more isolated, measurements deviating >2% from the linear fit in other filters at other times (e.g. F225W MJD∼56500, F275W MJD∼55750, and MJD∼56600, as well as two low points in F336W). There is some indication however, that the dips may be due to chip features in the UV which are not fully corrected by the current flat fields.

The UV flatfields exhibit prominent 'crosshatching' structures (see Section 11 in Mack *et al*. 2013). These features, a result of the annealing process applied during chip manufacture, are strongest in the bluest filters (± 2-3%), and are most pronounced on chip 1. In the monitor data, the star never lands exactly on the same location within the subarray; it drifts slightly from exposure to exposure, causing it to fall on and off the CCD's crosshatching artifacts. Indeed, in the UV there is more scatter in the countrates on chip 1 than on chip 2, consistent with the difference in crosshatch strength between the two chips.

Improvements to the UV flatfields are currently underway. Reanalysis of the contamination data using preliminary new flatfields for F218W and F225W shows considerable reduction in the extreme outliers in the dips: most delta flux values larger than ∼2% disappear. However, the overall scatter in the UV contamination data, as well as the longterm flux trends, remain. We note that the chip structures in redder filters, such as F606W and F814W, are intrinsically much smoother than those in the UV (Sabbi 2009) and thus the flatfields are unlikely to be a source of the overall scatter observed at longer wavelengths.

4.2. Longterm Trends

Table 4 summarizes the trend in flux percent change per year as a function of filter for the full dataset (June 2009 - Mar. 2014). Using all ∼five years of available on-orbit data, the UV photometry appears stable to ∼0.1%. Filters F438W and redward, however, show a downward trend in overall throughput, about 0.2-0.3% per year. With the exception of F850LP, the decline in throughput is higher on chip 1 than on chip 2.

Given the large amount of scatter in the pre-55500 MJD (Oct. 2010) data, we also did a linear fit on only the data taken after that date, shown in Figures 5 and 6, and tabulated in Table 5. Based on this partial dataset (the last ∼3.5 years), the photometry in all filter/chip

combinations show a decline over time. The decline ranges from a low of ∼0.1% per year in F275W on chip 1 to a high of ∼0.6% per year in F547M on chip 1. As for the full dataset, the declines are typically steeper on chip 1 than on chip 2.

We calculate formal errors for the flux percent change per year. We also perform Monte Carlo simulations, in which half of the datasets are randomly selected and from them a slope is calculated. For each filter a slope is calculated from a new random subset of the data 10,000 times. From these 10,000 runs we obtain an average and standard deviation for the slope of flux percent change versus time. These values are listed for each filter-amplifier set in Tables 4 and 5 The results of the runs were nearly Gaussian; see, for example, Figures 9 and 10.

Finally we plot the filters' pivot wavelength against slope for the full (Figure 7) and partial (Figure 8) datasets. It is interesting to note that ACS/WFC shows a similar trend to WFC3/UVIS for sensitivity plotted against pivot wavelength (see Bohlin, Mack, & Ubeda 2011): both detectors show a sensitivity dip between 4000 and 7000 angstroms. Before Servicing Mission 4 (SM4), ACS/WFC showed a comparable declining trend in sensitivity, of ∼0.04 % per year (Ubeda & Anderson 2013), which has become negligible since SM4. Another study reported a less than ∼0.3 % per year loss prior to SM4 in all filters except the short-wavelength filters F220W and F250W (Bohlin, Mack, & Ubeda 2011). This trend in ACS/WFC is similar to the trend in WFC3/UVIS that we have detailed in this report. ACS/WFC and WFC3/UVIS are both two-chip CCD detectors and have similar shutters and filters, and it is possible the cause for their sensitivity declines lie in their common components.

The cause for these downward trends in both WFC3/UVIS and ACS/WFC, however, remains unclear. We have investigated and ruled out the following effects for UVIS.

- CTE. We expect the effects of charge transfer efficiency (CTE) loss to be minimal because our images are on the corners of the detector near the amplifiers (where CTE loss is smallest), our aperture is large (10 pixel radius), our source star is bright (flux counts in the 250,000-400,000s, on average, for all the filters), and our backgrounds are higher than a few electrons. To test our assumptions, we performed two tests. First, we have compared the flux counts of F225W, amplifier C, measured on CTE-corrected and non-CTE-corrected images (see `http://www.stsci.edu/hst/wfc3/ins_performance/CTE/` for the pixel-based CTE correction software). We found that the differences between CTE-corrected and non-CTE-corrected flux counts is on the order of 10^{-4}. As another means of assessing the effect of CTE losses on our photometry, we use the CTE model (Noeske 2012) with the most up-to-date coefficients to estimate the decrease in CTE that we would expect in our images. There may be

a mild trend of increasing CTE loss for bright sources in low background exposures at the level of ∼1% over two years (Noeske, priv.comm.). These results are for sources 2048 pixels from an amplifier and radius 3 pixel aperture. The data in this ISR are ∼100 pixels from the amplifier and use 10 pixel aperture. Therefore, the estimated CTE losses for our standard white dwarf are 1% / (2048/100) = 0.05% in two years = 0.025 in one year, assuming a radius 3 aperture. For radius 10, the CTE losses would be even lower, << 0.02%/year. From these two tests we conclude that the effects of CTE loss are negligible in our images.

- Breathing. This is focus change on the timescale of an orbit due to temperature-induced spatial variations between the HST secondary and primary mirrors. The typical spatial variation per orbit is several microns (Dressel 2012). The effect of breathing on the encircled energy over different apertures on the WFC3 filter F410M has been examined by L. Dressel (2012). In the largest diameter aperture (0.25 arc sec) studied, the fraction of encircled energy changed only by 1 - 2% across the full span of −4 microns to +6.5 microns measured focus. Because our aperture diameter is significantly larger - 0.8 arcsec - breathing's impact on our photometry should be negligible.

- Flat field. Reprocessing with non-flat fielded data did not significantly change the slopes. Structures in the UV flat fields can not be a cause since the decline is present, and at higher levels, in the redder filters.

- Pixel area map and cosmic-ray flagging. Redoing the photometry with non-PAM-corrected data did not change the slopes significantly. And as discussed in Subsection 4.1, we have validated that `LACOSMIC` is performing well.

- Filters. The filters being used are constructed from a variety of materials using different production methods. It is highly unlikely that the throughput changes in the monitoring data are due to degradation in the filters.

- Absolute gain. This would be a likely candidate for causing longterm throughput changes seen in many filters. However, if the gain were drifting over time, the photometry in all filters should be declining. Instead, in both the full and partial datasets, the UV filters show no or little trend, respectively, while the red filters exhibit the largest change over time. The absolute gain measurements to date have shown the gain to be stable to 1-2% over five years (Gunning & Baggett 2014).

- Relative gain. Given the sparse time-sampling of the absolute gain (measured ∼two times per year) we made use of a more frequently-sampled dataset, the bowtie monitor,

to investigate whether the relative gains of the amps may be drifting. The bowtie monitor has been acquiring binned internal flat fields (intflats) since the installation of WFC3 into HST. A full description of the program and its standard analysis are available in Bourque & Baggett (2013). For the purposes of evaluating the relative gain, we use the unsaturated intflats from the bowtie monitor. These were acquired initially twice a day, a frequency gradually reduced to the current sampling of two unsaturated intflats every three days. Relative to quadrant A, flat field count rates in quadrants B and C show a very slight decrease with time ($\sim$0.05% over $\sim$1500 days), while count rates in quadrant D, relative to A, show a very slight increase with time ($\sim$0.03% over $\sim$1500 days). Assuming these drifts are not due to, for example, changes in the flat field lamp, the levels are significantly lower than that observed in the photometry.

- Readnoise. Drifting of the readnoise levels in WFC3 over time is unlikely to be able to cause the changes seen in the photometric throughput over time, particularly given the differences in the trends with filter. Nevertheless, we analyzed readnoise levels in on-orbit biases and confirmed that the UVIS readnoise values have been stable on-orbit, with values of 2.93, 3.01, 2.92, and 3.04 e-/pix and standard deviations of 0.03, 0.01, 0.02, 0.02, for quadrants A, B, C, and D, respectively.

- Sky correction. The fluxes with and without sky correction are almost identical, both showing the downward trend.

- Instrument stability. The health of the instrument is routinely monitored by STScI engineers using a variety of continuously-collected telemetry data (e.g., detector and housing temperatures, electronics box temperatures and voltages, clock, gate, and drain voltages, etc.). WFC3 has been stable over its lifetime on-orbit, and no anomalous excursions have been detected which could account for the observed photometric trends.

5. Contamination

The presence of contamination, such as on the CCD window, would likely cause a decline in photometric throughput. UV wavelengths are particularly sensitive to contaminants, and therefore, we would expect any effects to manifest first in the short-wavelength filters. The Wide Field Planetary Camera 2 (WFPC2) on HST, for example, with its cold CCD window, was susceptible to contamination buildup, and as a result, exhibited declines in UV throughput (see Section 5.2 in Gonzaga *et al.* 2010). In that case, the situation was successfully controlled via routine decontamination procedures that warmed the windows, removing the contaminants.

On WFC3, the CCD windows are kept warm but other optical elements are not (e.g. pick-off mirror) and thus could conceivably be at risk for acquiring contaminants. An initial assessment of WFC3 using the UV grism G280 showed no reduction in UV throughput, but instead there appeared to be an increase in flux at bluer wavelengths (2-5% over ∼1 year, though error bars are large: 4-9%; see Rothberg, Pirzkal, & Baggett 2011).

Our standard star observations in F218W, F225W, and F275W provide a complementary long-term dataset with which to check for contamination effects. If present, we should see stronger declines in the UV throughput compared to declines in the red throughput. In fact, we see the reverse: more decline with the redder filters than with the bluer filters. We speculate that there may be an underlying slow, uniform decline in throughput across all wavelengths that is being offset somewhat in the UV filters, resulting in shallower declines at the blue end.

6. Conclusions

We see no evidence of contamination in the UVIS channel. There are slight longterm trends in the photometric throughput, a 0.2-0.3% decline per year over the full five years in the red filters, and less in the UV. The declines are somewhat higher if measured from the last ∼3.5 years, ranging from a low of ∼0.1% per year (F275W, chip 1) to a high of ∼0.6% per year (F547M, chip 1). In both the full and partial datasets, the declines are steeper in chip 1 than in chip 2.

7. Future Work

The cause for the photometric trends remains unclear, but further investigation is underway. Regardless, the accumulated change over time is significant enough, especially in the redder filters, that corrections will need to be provided for the photometric zeropoints. Future work will include continuation of the photometric monitoring and implementing time-dependent zeropoints. In addition, new UV flat fields are anticipated for later in 2014 (Mack, priv.comm.). We will use them on the monitor data, though for the reasons enumerated above, we do not expect our results to change substantially. We want to analyze the new G280 data taken since 2011 to determine whether any further conclusions can be drawn concerning the photometric throughput behavior over time in the UV. Finally, since their sensitivity declines are similar, we plan to look into elements common between ACS/WFC and WFC3/UVIS in search for a cause for the photometric trends. In particular, we will

investigate the evolution of the performance of WFC3/UVIS's shutter.

8. Acknowledgments

We would like to thank John MacKenty for insightful discussions and Adam Riess for reviewing this ISR. We would also like to thank Kai Noeske for working with us to quantify the effects of CTE loss.

References

Bohlin, R., 1996, "Spectrophotometric standards from the Far-UV to the near-IR on the white dwarf flux scale"

Bohlin, R. C., Mack, J., & Ubeda, L., 2011, ACS ISR 2011-03: "Flux Calibration of the ACS CCD Cameras: III. Sensitivity Changes Over Time"

Bourque, M. & Baggett, S., 2013, WFC3 ISR 2013-09: "WFC3/UVIS Bowtie Monitor"

Dressel, L., 2012, WFC3 ISR 2012-14: "Breathing, Position Drift, and PSF Variations on the UVIS Detector"

Gonzaga, S., & Biretta, J. et al., 2010, HST WFPC2 Data Handbook, v. 5.0, ed.

Gunning, H., & Baggett, S., 2014, WFC3 ISR 2014-05: "WFC3 Cycle 20 Proposal 13168: UVIS Gain"

Kalirai, J. et al., 2009, WFC3 ISR 2009-31: "WFC3 SMOV Proposal 11450: The Photometric Performance and Calibration of WFC3/UVIS"

Kalirai, J., Baggett, S., Borders, T., & Rajan, A., 2010, WFC3 ISR 2010-14: "The Photometric Performance of WFC3/UVIS: Temporal Stability Through Year 1"

Mack, J., Sabbi, E., & Dahlen, T., 2013, WFC3 ISR 2013-10: "In-flight Corrections to the WFC3 UVIS Flat Fields"

Noeske, K et al., 2012, WFC3 ISR 2012-09: "WFC3 UVIS Charge Transfer Efficiency October 2009 to October 2011"

Rothberg, B., Pirzkal, N., & Baggett, S., 2011, WFC3 ISR 2011-18: "First Results from Contamination Monitoring with the WFC3 UVIS G280 Grism"

Sabbi, E., 2009, WFC3 ISR 2009-19: "WFC3 SMOV Program 11452: UVIS Flat Field Uniformity"

Stys, D., & Walborn, N., 2001, STIS ISR 2001-01: "Sensitivity monitor report for the STIS first-order modes-III"

Ubeda, L. & Anderson, J., 2013, ACS ISR 2013-01: "Study of the evolution of the ACS/WFC sensitivity loss"

van Dokkum, P. G., 2001, PASP, 113, 1420

Whitmore, B., Heyer, I., & Baggett, S., 1996, WFPC2 ISR 1996-04: "Effects of contamination on WFPC2 photometry"

		Amp A				Amp C			
Filter	*Obs. Period*	*% Change/Year*	*Formal Error*	*Average*	*Stand. Dev.*	*% Change/Year*	*Formal Error*	*Average*	*Stand. Dev.*
F218W	6/2009 - 3/2014	0.164	0.000	0.171	0.036	0.084	0.000	0.086	0.028
F225W	6/2009 - 3/2014	0.082	0.000	0.121	0.045	0.016	0.000	0.084	0.034
F275W	6/2009 - 3/2014	−0.031	0.000	−0.027	0.040	0.012	0.000	0.008	0.035
F336W	6/2009 - 3/2014	−0.007	0.000	−0.007	0.044	0.001	0.000	0.019	0.050
F390M	6/2009 - 10/2012	−0.288	0.000	−0.252	0.093	−0.010	0.001	0.144	0.107
F390W	6/2009 - 10/2012	−0.167	0.000	−0.174	0.083	−0.157	0.000	−0.110	0.081
F438W	6/2009 - 3/2014	−0.199	0.000	−0.207	0.040	−0.168	0.000	−0.161	0.051
F467M	6/2009 - 10/2012	−0.338	0.001	−0.324	0.103	−0.180	0.001	−0.014	0.088
F475W	8/2009 - 10/2012	−0.382	0.000	−0.294	0.070	−0.242	0.000	−0.214	0.102
F547W	8/2009 - 10/2012	−0.360	0.000	−0.259	0.072	−0.227	0.001	−0.176	0.096
F555W	11/2010 - 10/2012	−0.250	0.001	−0.407	0.152	−0.160	0.001	−0.203	0.181
F606W	6/2009 - 3/2014	−0.350	0.000	−0.360	0.038	−0.322	0.000	−0.322	0.057
F814W	6/2009 - 3/2014	−0.163	0.000	−0.158	0.061	−0.134	0.000	−0.129	0.037
F850LP	11/2010 - 10/2012	−0.076	0.001	−0.207	0.220	−0.199	0.001	−0.150	0.239

Table 4: *Percent change in flux throughput per year for the the full datasets (June 2009 to March 2014). The second column gives the time period over which the data were taken. The third and seventh columns list the linear fit slopes of percent changes in amplifier quadrants A and C, found using* `IRAF/TLINEAR` *and weighted by the uncertainty in the flux ratio. The formal uncertainty in the slopes, listed in the fourth and eighth columns, is as given from* `IRAF/TLINEAR`*. The fifth and ninth columns list the average of 10,000 simulated slope percent changes per year. (See Section 4.2 for further discussion on the Monte Carlo analysis). Finally, the sixth and tenth columns list the standard deviation of the 10,000 simulations. See Figures 3 and 4 for corresponding plots.*

		Amp A				Amp C			
Filter	*Obs. Period*	*% Change/Year*	*Formal Error*	*Average*	*Stand. Dev.*	*% Change/Year*	*Formal Error*	*Average*	*Stand. Dev.*
F218W	11/2010 - 3/2014	−0.131	0.000	0.039	0.057	−0.265	0.000	−0.197	0.035
F225W	11/2010 - 3/2014	−0.170	0.000	0.002	0.075	−0.252	0.000	−0.144	0.052
F275W	11/2010 - 3/2014	−0.091	0.000	−0.044	0.059	−0.143	0.000	−0.137	0.040
F336W	11/2010 - 3/2014	−0.025	0.000	−0.032	0.067	−0.006	0.000	0.032	0.067
F390M	11/2010 - 10/2012	−0.404	0.001	−0.389	0.312	−0.320	0.001	−0.127	0.291
F390W	11/2010 - 10/2012	−0.239	0.001	−0.360	0.267	−0.173	0.001	0.130	0.236
F438W	11/2010 - 3/2014	−0.207	0.000	−0.186	0.060	−0.220	0.000	−0.206	0.066
F467M	11/2010 - 10/2012	−0.377	0.001	−0.382	0.260	−0.398	0.001	−0.194	0.273
F475W	11/2010 - 10/2012	−0.508	0.001	−0.301	0.202	−0.248	0.001	−0.112	0.187
F547W	11/2010 - 10/2012	−0.619	0.001	−0.711	0.143	−0.330	0.001	−0.256	0.215
F555W	11/2010 - 10/2012	−0.250	0.001	−0.408	0.152	−0.159	0.001	−0.208	0.181
F606W	11/2010 - 3/2014	−0.288	0.000	−0.340	0.063	−0.319	0.001	−0.374	0.109
F814W	11/2010 - 3/2014	−0.304	0.001	−0.232	0.131	−0.248	0.000	−0.249	0.041
F850LP	11/2010 - 10/2012	−0.078	0.001	−0.210	0.219	−0.198	0.001	−0.150	0.232

Table 5: *Percent change in flux throughput per year for the partial datasets (November 2010 to March 2014). Notice the linear fits for blue filters (F218W, F225W, and F275W) following November 2010 are all negative, whereas the fits of their full datasets are positive. See Table 4 for full description of columns, and Figures 5 and 6 for corresponding plots.*

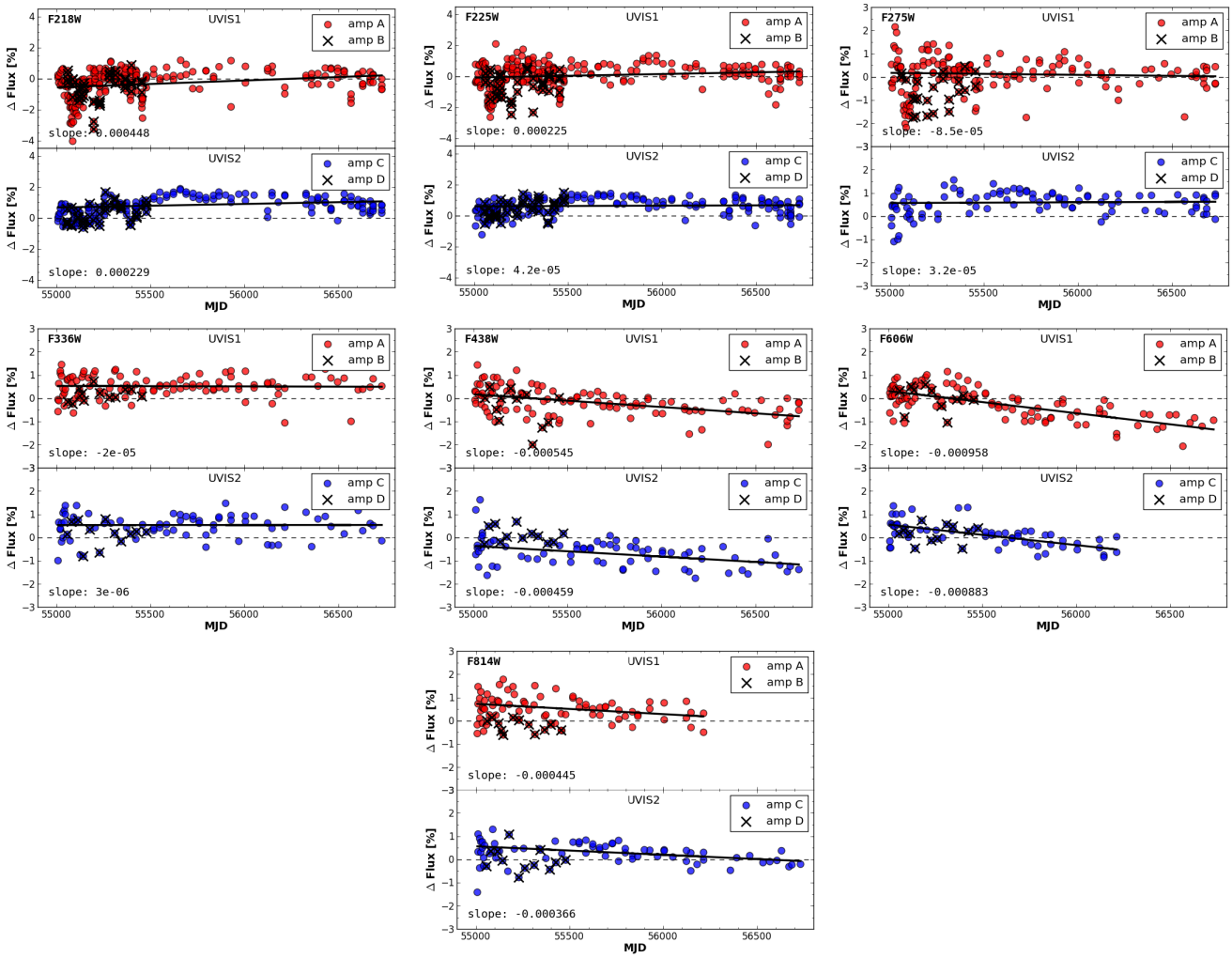

Fig. 3.— *The full datasets of the critical UV filters (F218W, F225W, F275W, F336W, and F438W) and control filters (F606W and F814W) that have had continuous coverage from SMOV (July - August 2009) to March 2014. On the y-axis is the countrate divided by the average countrate of the dataset's first three images, yielding a percent change in countrate, which we call* $\Delta Flux$*. On the x-axis is time in Modified Julian Date. The errorbars on* $\Delta Flux$ *are smaller than the plot points. The top halves plot the observations taken on UVIS chip 1 and the bottom halves plot the observations taken on chip 2. The chips are further subdivided by amplifier quadrant. Quadrants B and D have data extending from August 2009 to October 2010. Because this time range is so short, we do not attempt a linear fit on the B and D data. The fit lines and slopes apply only to quadrants A and C.*

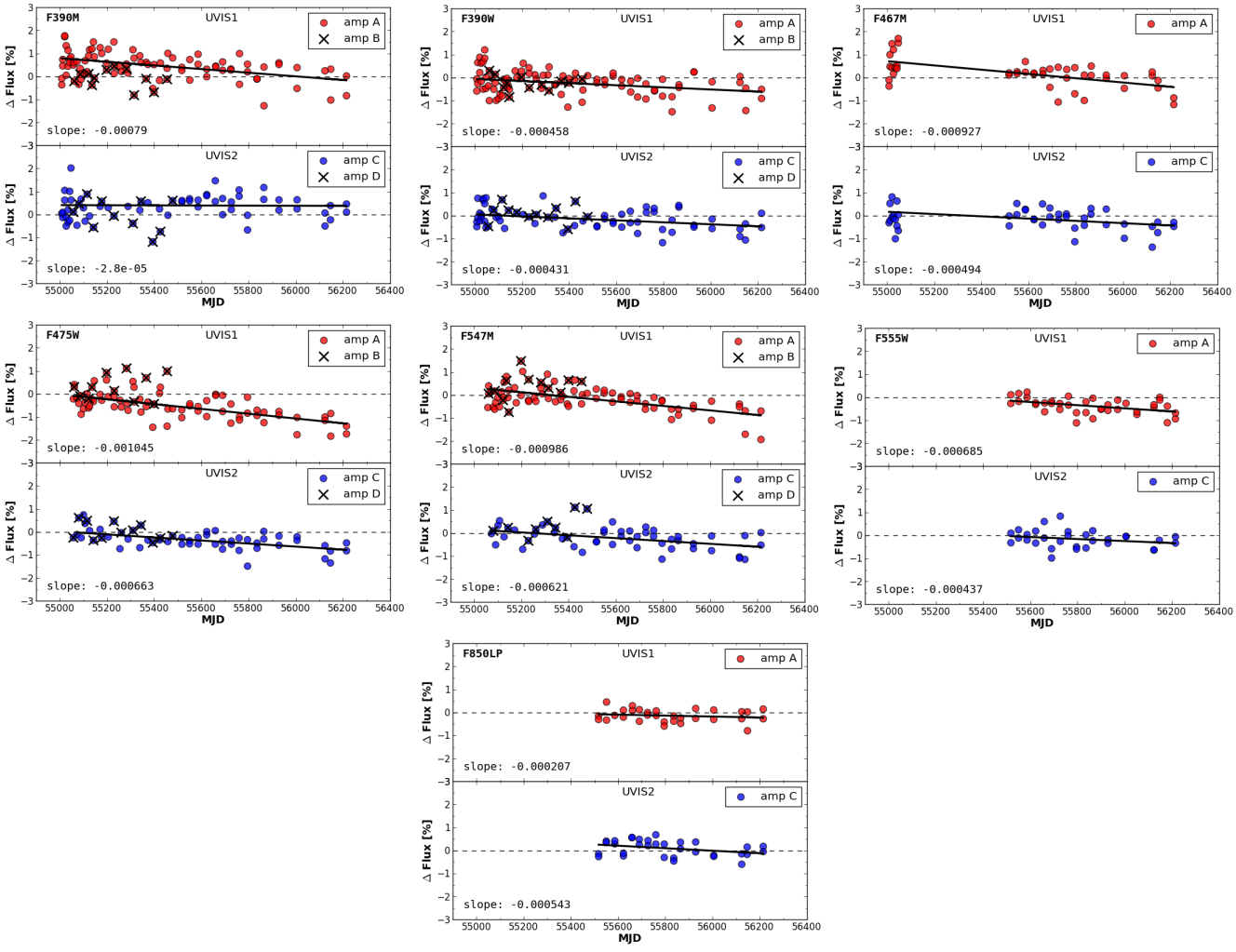

Fig. 4.— *The full datasets of the filters (F390M, F390W, F467M, F475W, F547M, F555W, and F850LP) whose coverage extends from either SMOV (July - August 2009) or October 2010, to October 2012. See Figure 3 for further description. These filters are less commonly used and mostly non-UV.*

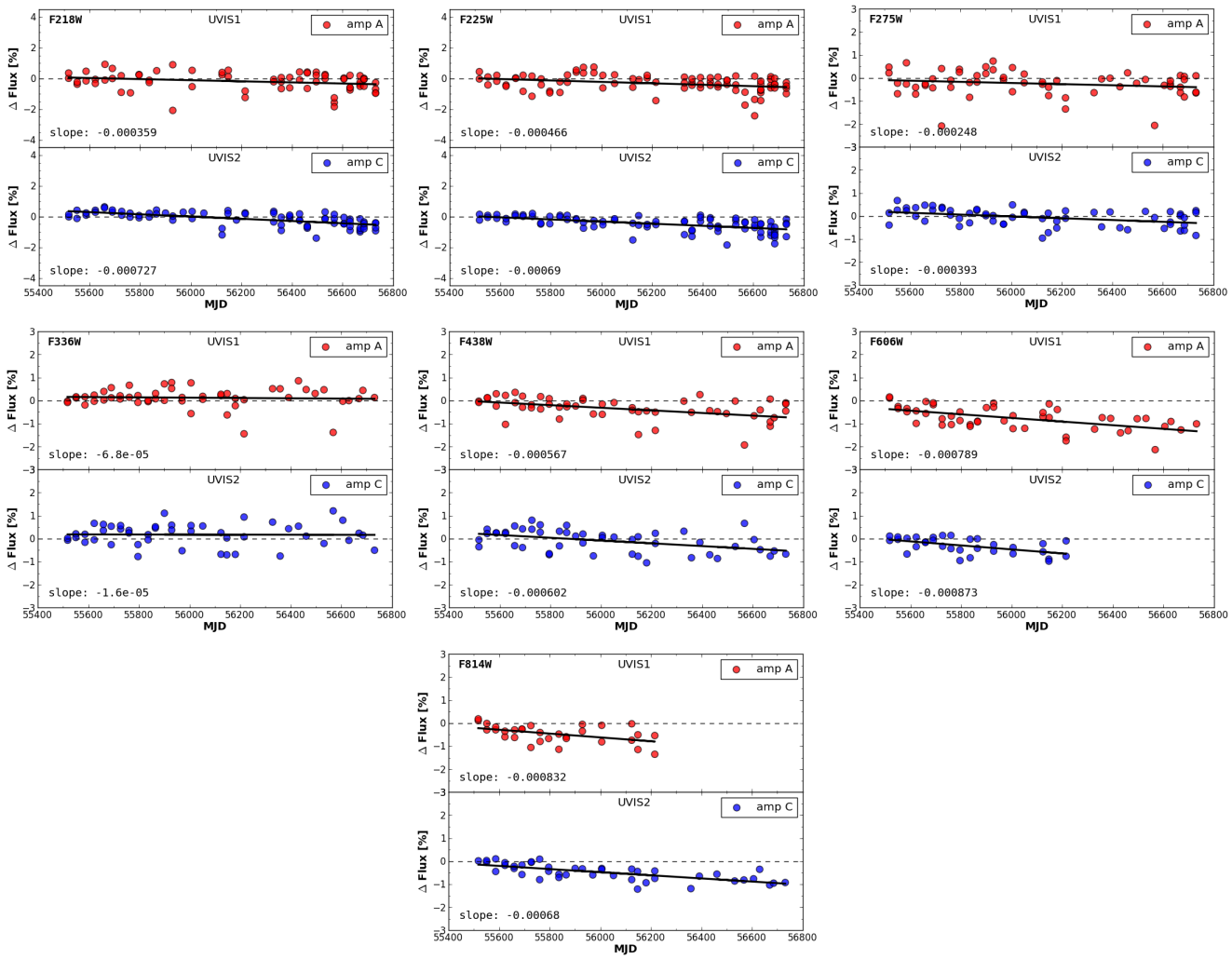

Fig. 5.— *The partial datasets, from MJD 55500 (October 2010) onward, of the filters that have had continuous coverage from SMOV to March 2014. See Figure 3 for further description.*

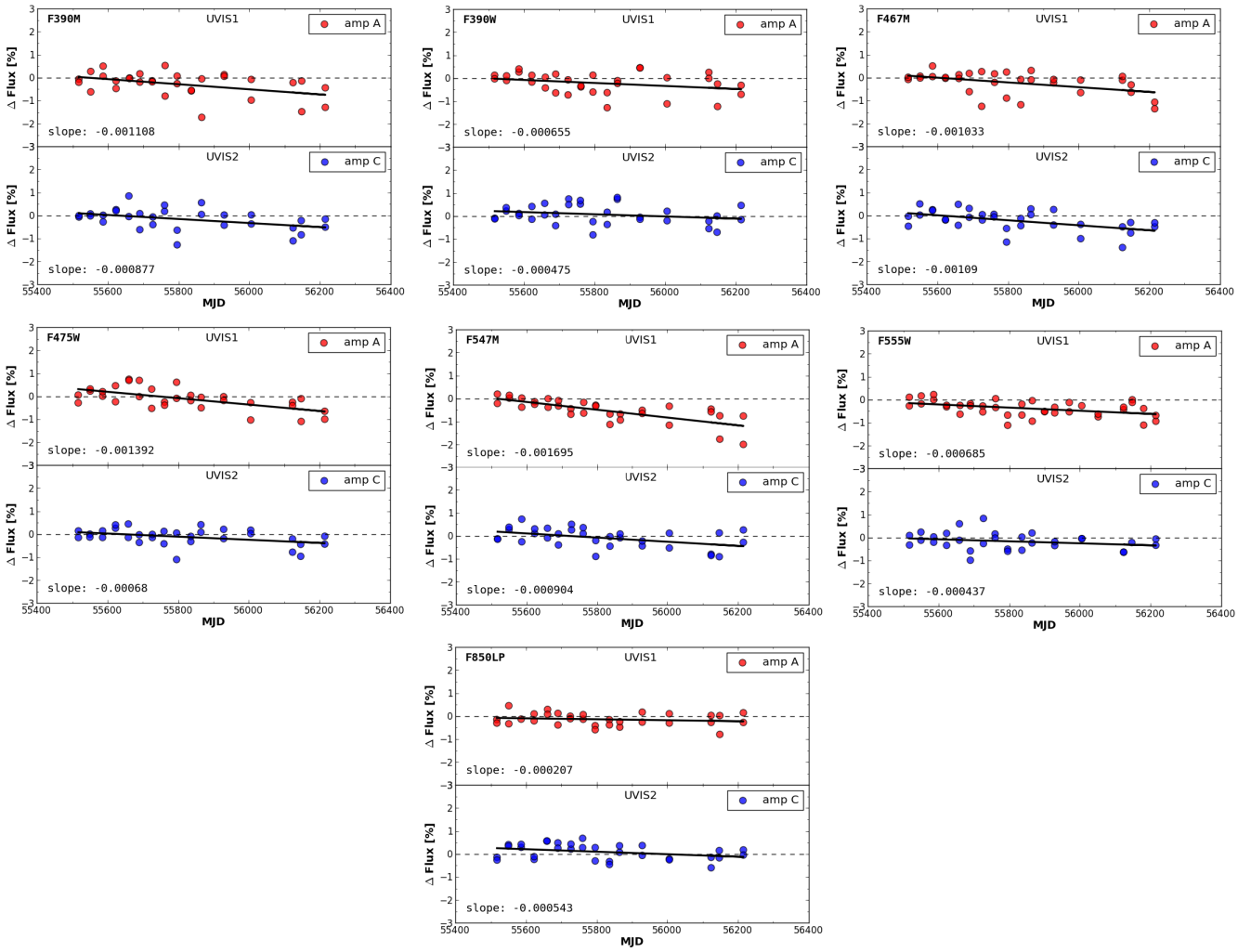

Fig. 6.— *The partial datasets, from MJD 55500 (October 2010) onward, of the filters that have had coverage from SMOV to October 2012. See Figures 3 and 4 for further description.*

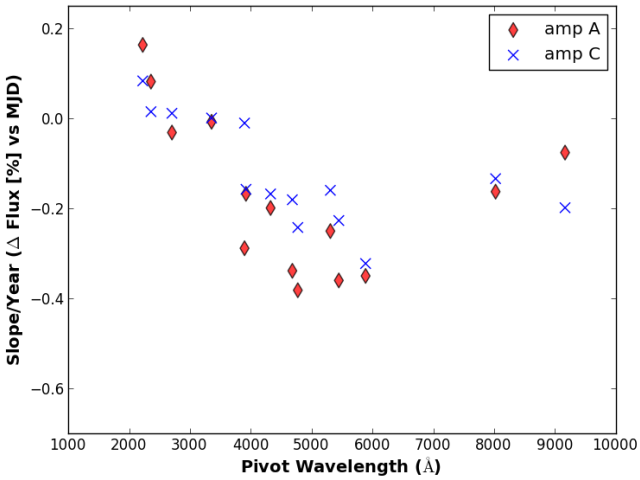

Fig. 7.— *The slopes per year of the full dataset (June 2009 to March 2014) plotted against the filters' pivot wavelength. See Table 4 for list of slopes*

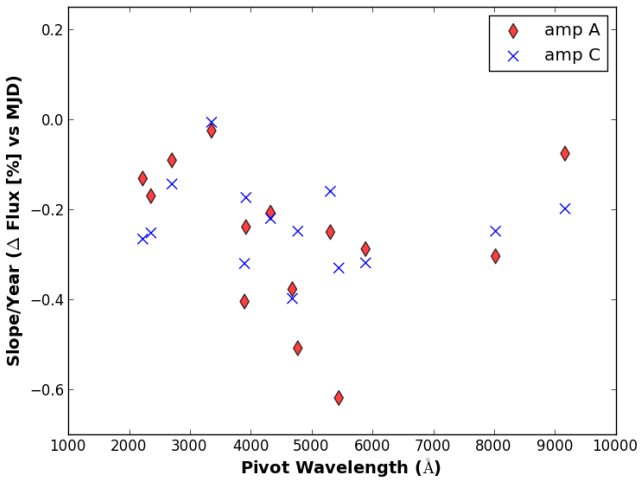

Fig. 8.— *The slopes per year of the partial dataset (October 2010 to March 2014) plotted against the filters' pivot wavelength. See Table 5 for list of slopes*

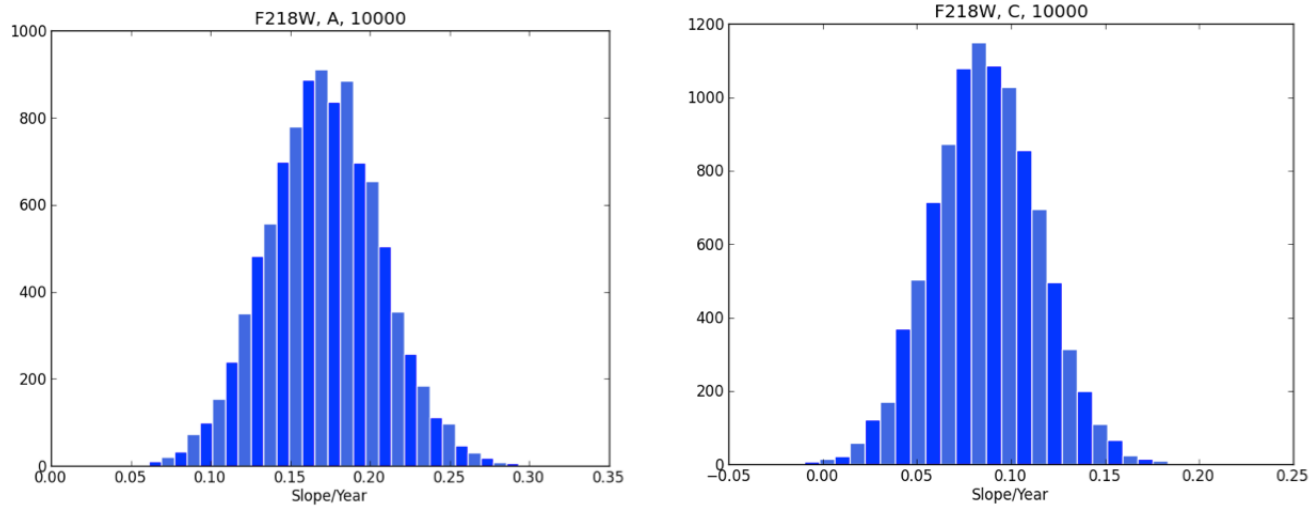

Fig. 9.— *Results for filter F218W, amplifiers A (left) and C (right) of 10,000 Monte Carlo simulations performed on the slope per year of percent flux change versus time. The distributions are approximately Gaussian.*

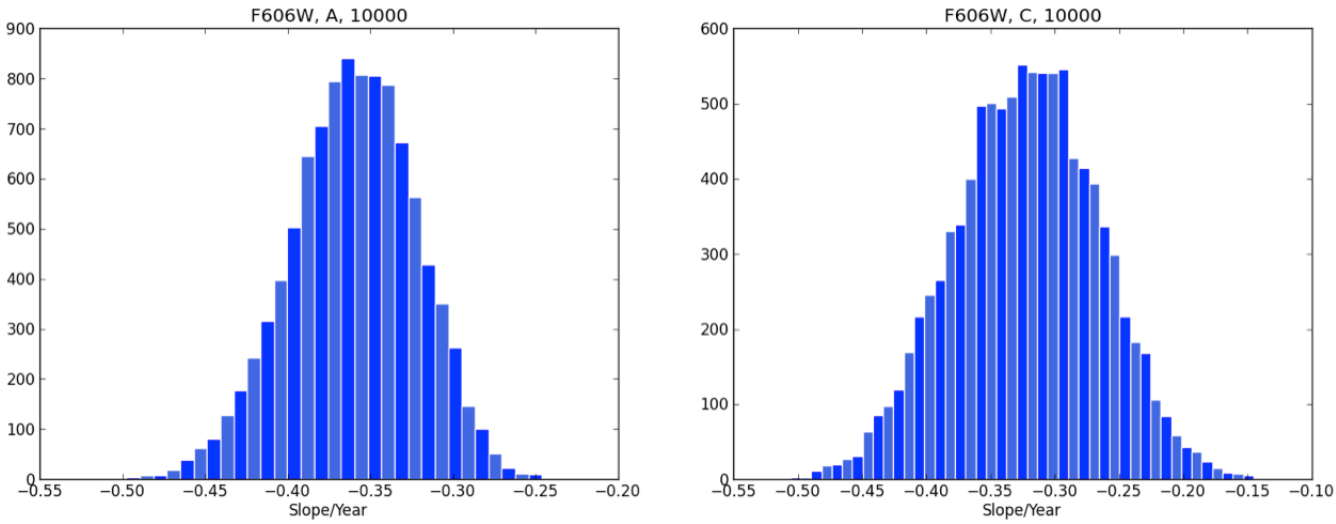

Fig. 10.— *Same as above, for filter F606W.*